Topological triple phase transition in non-Hermitian quasicrystals with complex asymmetric hopping

Shaina Gandhi [*] and Jayendra N. Bandyopadhyay [†]
Department of Physics, Birla Institute of Technology and Science, Pilani 333031, India

(Received 19 June 2023; revised 3 July 2023; accepted 7 July 2023; published 18 July 2023)

The triple phase transitions or simultaneous transitions of three different phases, namely, topological, parity-time ($\mathcal{PT}$) symmetry breaking, and metal-insulator transitions, are observed in an extension of the $\mathcal{PT}$ symmetric non-Hermitian Aubry-André-Harper model. In this model, besides the non-Hermitian complex quasiperiodic on-site potential, non-Hermiticity is also included in the nearest-neighbor hopping terms. Moreover, the nearest-neighbor hopping terms are also quasiperiodic. The presence of two non-Hermitian parameters, one from the on-site potential and another one from the hopping part, ensures $\mathcal{PT}$ symmetry transition in the system. In addition, tuning these two non-Hermitian parameters, we identify a parameters regime, where we observe the triple phase transition. Following some recent studies, an electrical circuit based experimental realization of this model is also discussed.

DOI: 10.1103/PhysRevB.108.014204

I. INTRODUCTION

In quantum mechanics, the Hermitian property of any observable not only ensures the measurement outcomes of that observable to be real, but it also preserves the total probability of all the outcomes. Over the past few years, systems with non-Hermitian Hamiltonians have become an important field of research [1–4]. The non-Hermitian Hamiltonians effectively represent quantum systems which exchange particles and/or energy with their environment [2,5]. The non-Hermiticity in the Hamiltonians leads to the complex energy spectra which is a signature of nonconservative systems. However, the non-Hermitian Hamiltonians with parity-time ($\mathcal{PT}$) symmetry have real eigenvalues [6–8]. Therefore, the $\mathcal{PT}$ symmetric Hamiltonians are considered as a more general class of Hamiltonians which allows loss and gain in the systems.

The spectral properties of the non-Hermitian systems show some strange behaviors under the presence of different symmetries, which has no Hermitian counterpart. One prominent example is that non-Hermitian Hamiltonians with $\mathcal{PT}$ symmetry host a typical special degeneracy, known as exceptional points, where the eigenvalues and the eigenvectors coalesce and thus the corresponding non-Hermitian matrices do not have a full basis of eigenstates [9–14]. Furthermore, the skin effect in non-Hermitian systems emerges from their inherent topology. This phenomenon refers to the localization of eigenstates near the system's boundary. This localization is a manifestation of the nontrivial topological properties of the system, which can be characterized using mathematical tools such as topological invariants [15,16]. Specifically, under open boundary conditions, the bulk states concentrate at the edges of the lattice, giving rise to the non-Hermitian skin effect. This phenomenon breaks the conventional bulk-boundary correspondence observed in Hermitian systems [17–19].

Previous investigations in the field of non-Hermitian quantum mechanics have provided valuable insights into the intriguing phenomena that arise when quantum-mechanical particles encounter randomness and non-Hermitian systems. A notable and extensively studied example in this realm is the non-Hermitian version of the celebrated Anderson model [20]. The non-Hermitian Anderson model has also been studied extensively [21–28]. Notably, Hatano and Nelson were pioneers in exploring the localization transitions in quantum-mechanical particles described by the non-Hermitian Anderson model with asymmetric hopping [21–23]. Their groundbreaking study revealed a localization-delocalization transition induced by the presence of the random potential, characterized by the emergence of complex eigenvalues in the system. Subsequently, the investigation of the non-Hermitian Anderson model expanded to include two-dimensional [25] and three-dimensional cases [26,28], providing further insights into the localization properties of the eigenstates. These models, unlike the Hatano-Nelson model, incorporated non-Hermiticity by introducing complex on-site random potentials.

In addition, there is another class of non-Hermitian models in one dimension, known as Aubry-André-Harper (NH-AAH) models [29–33]. The NH-AAH model physically represents one-dimensional (1D) quasicrystals with loss and gain processes. The quasicrystalline property and the non-Hermiticity are introduced into the system through an on-site quasiperiodic potential by a complex phase factor. The Hermitian counterpart of this model shows metal-insulator (MI) transition determined by a fixed ratio of the strength of the on-site quasiperiodic potential and the nearest-neighbor hop-

[*] p20200058@pilani.bits-pilani.ac.in
[†] jnbandyo@gmail.com

 ©2023 American Physical Society

ping strength [34]. Besides this ratio, the MI transition in the NH-AAH model with $\mathcal{PT}$ symmetry also depends on the imaginary part of the complex phase. Very interestingly, a recent study has found that the NH-AAH model preserves $\mathcal{PT}$ symmetry when the system is in the metallic phase. This implies that at the MI phase transition point, the $\mathcal{PT}$ symmetry in the NH-AAH model spontaneously breaks down via exceptional points and complex energy eigenvalues start appearing [21,22,35]. Moreover, it is worth noting that at the dual transition point where both the MI phase transition and the $\mathcal{PT}$ symmetry breaking occur, the NH-AAH model exhibits an additional topological phase transition [36]. This combination of three simultaneous phase transitions, often referred to as the "*triple*" phase transition, has attracted significant interest in the field. Furthermore, experimental realizations of this triple phase transition have been reported [37], providing further validation of the theoretical predictions. These three phase transitions have completely different underlying physics: (a) The MI transition is determined by the strength of disorder in the system; (b) the $\mathcal{PT}$ symmetry breaking leads to a real to complex energy spectrum, and (c) the topological phase transition is determined by the loss of adiabatic connection of the Hamiltonian at the transition point. The non-Hermiticity is responsible for this rare event in the NH-AAH Hamiltonian.

Recently, a non-Hermitian version of the AAH model with $\mathcal{PT}$ symmetry is proposed [38]. In this model, the non-Hermiticity is introduced via asymmetric complex hopping. This model shows concurrent transitions of MI and $\mathcal{PT}$ symmetry. These phase transitions are robust against the system's size and the on-site disorder represented by incommensurate (quasiperiodic) potential. In Ref. [39], another version of the non-Hermitian AA model was proposed. In this model, the non-Hermiticity was introduced at on-site quasiperiodic potential, as well as at the nonreciprocal hopping. Here, the interplay of the non-Hermiticity and the disorder captures a new physical aspect. For any values of the system's parameters, this model is not $\mathcal{PT}$ symmetric. The presence of two non-Hermitian parameters is responsible for this non-$\mathcal{PT}$ symmetric nature of the model. As a consequence, the triple phase transition cannot be observed in this model.

The aim of this paper is to propose a NH-AAH model with $\mathcal{PT}$ symmetry while incorporating two non-Hermitian parameters. The two non-Hermitian parameters are introduced in two ways: the standard on-site quasiperiodic potential with a complex phase factor, and an incommensurately modulated complex asymmetric hopping. Remarkably, this system exhibits a triple phase transition within a specific regime of the system's parameters.

This paper is organized as follows: Section II provides an introduction to the model, including its general properties. Section III focuses on the phase diagram and analyzes the triple phase transition. Specifically, it examines the topological transition, PT symmetry breaking, and MI transitions. Section IV delves into the eigenspectra analysis, focusing on the triple phase transition for a specific chosen value of the non-Hermitian parameter. In Section V, the paper discusses the experimental realization of the model, providing insights and information on relevant references. Finally, we summarize the work in Sec. VI.

II. MODEL HAMILTONIAN AND PROPERTIES OF ITS EIGENSTATES

The tight-binding Hamiltonian of this NH-AAH model is

$$\begin{aligned} H = \sum_{j=1}^{L} & V\cos(2\pi\beta j + \phi_1 + \phi_2)\hat{c}_j^\dagger \hat{c}_j \\ & + [t + i\gamma\ \sin(2\pi\beta j + \phi_1)]\hat{c}_{j+1}^\dagger \hat{c}_j \\ & + [t + i\gamma\ \sin(2\pi\beta(j+1) + \phi_1)]\hat{c}_j^\dagger \hat{c}_{j+1}, \end{aligned} \tag{1}$$

where the phase factors are $\phi_1 = \pi - \pi\beta \pmod{2\pi}$ and $\phi_2 = \theta - ih$. The number of lattice sites is L. With this choice of the parameter ϕ_1 [38] and setting $\theta = 0$, the above Hamiltonian becomes $\mathcal{PT}$ symmetric. The space-reflection operator $\hat{P}$ and the time-reversal operator $\hat{T}$ have the following effects: $\hat{P}^{-1}\hat{c}_j\hat{P} = \hat{c}_{L+1-j}$, and $\hat{T}^{-1}i\hat{T} = -i$. We have provided a detailed analytical demonstration of the $\mathcal{PT}$ symmetry of our model in the Supplemental Material (SM) [40]. Here, the parameters h and γ respectively determine the strength of the non-Hermiticity at the on-site potential and hopping. Here, the on-site potential is modulated by a cosine function of strength V with periodicity $\frac{1}{\beta}$. The second and third terms of the Hamiltonian describe the complex asymmetric hopping.

We chose to set the parameter β in our study to be equal to σ_G, which is the inverse of the golden mean. This choice of β is a popular and commonly used option in research on the AAH model. The golden mean, as well as its inverse σ_G, satisfy diophantine condition. The best diophantine (rational) approximation of σ_G is the ratio of two consecutive numbers of the Fibonacci series $\{f_n\}$ and the approximation becomes better with increasing n, i.e., $|\sigma_G - \lim_{n\to\infty}(f_{n-1}/f_n)| \to 0$. The Fibonacci series is obtained from the recursion relation $f_n = f_{n-1} + f_{n-2}$, with initial values $f_0 = 0$ and $f_1 = 1$. The above diophantine approximation of σ_G allows us to consider the following standard practice for the numerics. We set $\beta = f_{n-1}/f_n$ with a sufficiently large n and assume the number of lattice sites $L = f_n$. This approximation not only ensures the quasiperiodicity of the on-site potential for a finite number of lattice sites, but also makes the dual transformation to the Fourier transformed space exact [41]. Therefore, in our study, we set $\beta = \frac{144}{233}$, where 144 and 233 are consecutive Fibonacci numbers, and fix the number of lattice sites $L = 233$ throughout this study.

The Hermitian version of our model (i.e., when $\gamma = h = 0$) with irrational β shows the MI transition at the critical point $V = 2t$. For $V < 2t$, the system is metallic, whereas for $V > 2t$ the system becomes an insulator. In the case of the single parameter non-Hermitian case with $\gamma = 0$ and $h \neq 0$, the system is self-dual. This self-duality is manifested by the eigenfunctions having identical distributions in both real and momentum spaces, indicating an effective mapping between the Hamiltonian and its Fourier transform. Exploiting this self-duality, the critical point of the MI transition was analytically calculated as $h = \ln(\frac{2t}{V})$ for the NH-AAH model with a complex on-site potential [36]. As mentioned earlier that this critical point is the triple phase transition point, i.e., the simultaneous transition point for the MI transition, the

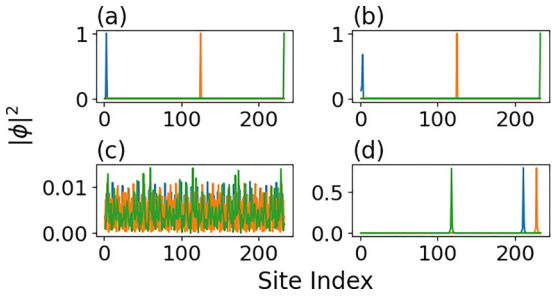

FIG. 1. Typical nature of the eigenstates corresponding to the Hamiltonian given in Eq. (1) with the OBC (top) and the PBC (bottom) are compared for the number of lattice sites $L = 233$. (a),(b) The top row shows three randomly picked eigenstates under the OBC that are all localized at some lattice site for both $h = 0.4$ and $h = 1.2$, respectively. (c),(d) The same eigenstates are presented in the bottom figure with the PBC, where all the eigenstates are extended for $h = 0.4$, but are localized at different lattice sites for $h = 1.2$.

$\mathcal{PT}$ transition, and the topological phase transitions. Unlike the NH-AAH model, where the non-Hermiticity is introduced solely through a complex on-site potential, our model described by the Hamiltonian given in Eq. (1) incorporates both complex sinusoidal asymmetric hopping terms and complex on-site potential. As a result, non-Hermiticity arises in two distinct parameters. Due to this additional complexity, our model does not exhibit self-duality. Hence, analytically we cannot find the transition point for this model. Therefore, the phase transition and other properties of this model are studied numerically. Furthermore, unlike the Hatano-Nelson model with non-Hermiticity in the off-diagonal disorder [21,22] and the NH-AAH model with non-Hermitian on-site quasiperiodic potential [37], our model has non-Hermiticity in both on-site potential and in nearest-neighbor hopping.

The prime focus of this paper is to explore the existence of triple phase transition in the presence of two non-Hermitian parameters. The eigenstates of this system are presented in Fig. 1. The eigenstates have revealed interesting insights about the behavior of the NH-AAH model. Here, we set the parameters $\gamma = 0.05$, $t = 1.0$, and $V = 1.0$. Specifically, we observe that the eigenstates of the system are primarily localized when open boundary condition (OBC) is imposed. This is illustrated for $h = 0.4$ in Fig. 1(a), and for $h = 1.2$ in Fig. 1(b). However, for the periodic boundary condition (PBC), we observe the effect of MI transition in the system. Here, in the metallic regime when the parameter $h = 0.4$, we observe extended eigenstates as shown Fig. 1(c). On the other hand, in Fig. 1(d), we show that in the insulating regime with $h = 1.2$, all the eigenstates are localized. These extreme boundary-condition-sensitive behaviors of the eigenstates are attributed to the interplay of the disorders due to the on-site quasiperiodic potential and the presence of the non-Hermiticity in the system.

III. ANALYSIS OF PHASE TRANSITIONS

First we study the variation of the transition point with the parameters γ and h, while the parameters V and t are fixed at unity, i.e., $V = t = 1.0$. We tune γ and h to identify

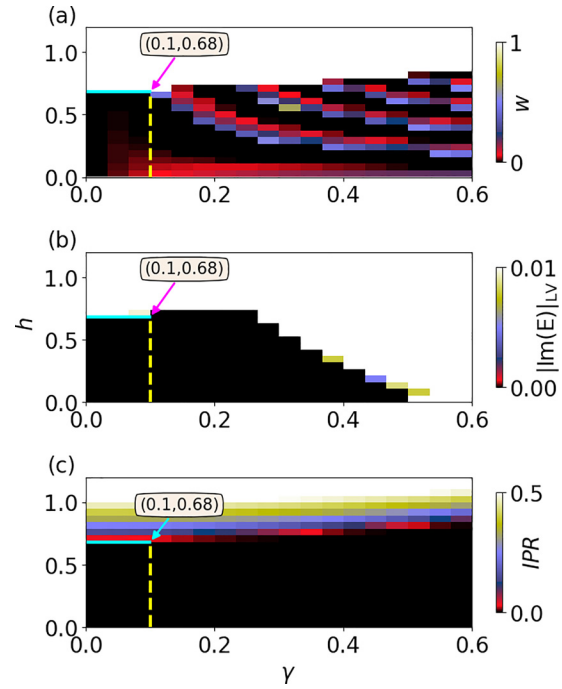

FIG. 2. The phase diagrams are presented for the topological, $\mathcal{PT}$ symmetry, and the MI transitions as the function of the parameters γ and h. (a) The topological phases are characterized by the calculation of the winding number w given in Eq. (2). The colors from black to white represent $w = 0$ to 1 values. The fluctuations in the winding number are less for $\gamma < 0.1$ (refer to color bar). In this region, the phase transition occurs at $h_c = 0.68$ as marked in the figure. (b) The largest value of imaginary parts of the energy eigenvalues are presented to observe the $\mathcal{PT}$ symmetry transition. The different color palettes separate the real and complex regions of the energies (refer to color bar). The $\mathcal{PT}$ symmetry is preserved in the regime $\gamma < 0.5$. A common transition point is observed at $h_c = 0.68$ for $\gamma < 0.1$. (c) The maximum values of the inverse participation ratio are shown to track the MI transitions. The MI transitions are observed for the whole range of γ, but at different values of the parameter h. For $\gamma < 0.3$, the MI transition occurs at $h_c = 0.68$. The vertical yellow lines in all the figures are describing the parameter regime $\gamma < 0.1$, where the triple phase transition is possible to observe. The horizontal cyan line at $h = h_c = 0.68$ marks the triple phase transition points.

whether the triple phase transition is possible in our model. These results are shown in Fig. 2. In Fig. 2(a), the topological phase transition is presented using a winding number as the topological invariant. The winding number is calculated from the following relation [5,36,42]:

$$w(h,\gamma) = \lim_{L\to\infty} \frac{1}{2\pi i} \int_0^{2\pi} d\theta \frac{\partial}{\partial\theta} \ln\left[\det H\left(\frac{\theta}{L}, h, \gamma\right) - E_B\right]. \tag{2}$$

The winding number $w(h,\gamma)$ counts the number of times the complex spectral trajectory encircles the base energy E_B, when the real phase θ varies from 0 to 2π. Here, the Hamiltonian H with the PBC is considered and L is as usual the number of lattice sites. For our analysis, we have chosen $E_B = 0$ as the base energy. The strengths of the non-Hermitian

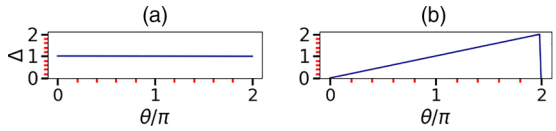

FIG. 3. The phase argument of $\det(H - E_B)$ versus θ is shown for $h = 0.6$ (left) and $h = 0.76$ (right) for $\gamma = 0.05$ and the number of lattice sites $L = 233$. As θ increases from 0 to 2π, the spectral trajectory does not encircle the base energy (left). Effectively, the spectrum of H does not wind. However, for $h = 0.76$, the spectral trajectory encircles the base energy once and the corresponding winding number is 1.

parameters decide the values of the winding number. We observe smooth topological phase transition identified by the transition of the winding number $0 \leftrightarrow 1$ in the parameter region $\gamma < 0.1$ marked by the vertical dashed-yellow line. For the non-Hermitian parameter $\gamma > 0.1$, fluctuations in the winding numbers are observed in the topologically trivial region. However, the topologically nontrivial region is still very well protected from the fluctuation in this parameter regime. In the parameter regime $\gamma < 0.1$, we find the critical point for the topological phase transition also at $h_c = 0.68$, which is shown by the horizontal solid cyan line.

This behavior of the winding number is further validated in Fig. 3, where we set the parameter $\gamma = 0.05$. Following Ref. [42], in this figure, the argument of determinant of the Hamiltonian $\Delta \equiv \arg[\det(H - E_B)]$ with respect to E_B is plotted as a function of the cyclic parameter θ while traversing θ for a full cycle of 0 to 2π. Here, we have selected two values of the parameter h: one is $h = 0.6$, less than the critical value h_c; and the other value is $h = 0.76$, larger than h_c. For $h = 0.6$, presented in Fig. 3(a), the winding number $w = 0$. Here, we observe that the trajectory of Δ does not enclose E_B while θ traverses a complete loop. On the other hand, for $h = 0.76$ where $w = 1$, the trajectory of Δ encircles E_B once as shown in Fig. 3(b).

Besides topological transition, we observe a simultaneous transition of the $\mathcal{PT}$ symmetry breaking as well as the MI phase transition. In Fig. 2(b), we show the $\mathcal{PT}$ symmetry transition. Here, we consider the largest value of the imaginary part of energy $|\mathrm{Im}(E)|_{\mathrm{LV}}$ as an indicator of the $\mathcal{PT}$ symmetry and study it as a function of the parameters γ and h. We find that, only in the regime $\gamma < 0.5$ (shown in black), the system has pure real eigenenergies. However, here the transition point varies with γ. Furthermore, we observe that, in the $\gamma < 0.1$ regime, the $\mathcal{PT}$ symmetry transition point is also at $h_c = 0.68$.

In Fig. 2(c), the MI transition is studied in the system investigating localization to delocalization transition of the eigenstates. We use the maximum inverse participation ratio (IPR) of the eigenstates as the measure of localization-delocalization transition. The IPR of a state is defined as

$$\mathrm{IPR} = \sum_n |\psi_n|^4 \Big/ \left(\sum_n (|\psi_n|^2\right)^2. \tag{3}$$

For the localized case, the IPR is larger and close to *unity*. On the other hand, for the delocalized or extended states, the IPR is proportional to the inverse of the dimension, where the dimension is the number of lattice sites $L = 233$. Therefore, for the extended or delocalized states (i.e., in the metallic regime), the IPR is very small. In the phase diagram, the metallic phase is represented by the black region and the (strongly) insulating phase region is represented by the white region. The other colors represent the critical regime. Here, we observe that the MI transition can occur for the whole range of γ, but at different values of h_c values. However, again for $\gamma < 0.1$, the transition point is at $h_c = 0.68$.

We infer from the phase diagrams of Fig. 2 that, in the regime $\gamma < 0.1$ and at $h_c = 0.68$, the system shows the triple phase transition. Thus, here we observe that, even in the presence of two non-Hermitian parameters, the system can show triple phase transitions. Based on these results, besides $V = t = 1.0$, we fix the parameter $\gamma = 0.05$ and continuously tune the parameter h to monitor the topological, $\mathcal{PT}$ symmetric, and MI transitions.

IV. ANALYSIS OF EIGENSPECTRA AND TRIPLE-PHASE TRANSITION

In Fig. 4(a), we display the real and imaginary parts of the eigenvalues for different values of h. Here we set the parameter $\gamma = 0.05$ to observe $\mathcal{PT}$ symmetry transition. For $h = 0.1$ and $h = 0.6$, eigenvalues are real and these show PT symmetry in the system. At the critical point $h = h_c = 0.68$, we observe the appearance of a tiny $[O(10^{-13})]$ nonzero imaginary part in the eigenvalues, which indicates breaking of the $\mathcal{PT}$ symmetry. For $h > h_c$, multiple looplike structures begin to form in the eigenvalues spectra. In the case of $h = 0.76$, we observe three loops in the spectrum that display the (multi)fractal property [43–48] as discussed in the SM [40]. As we further increase $h = 1.0$, 1.5, we observe gradual coalescence of multiple loops and the eventual formation of a single larger loop enclosing the origin. This presence of a single loop structure surrounding the origin indicates a tendency towards localization of the eigenstates. However, it does not necessarily imply full localization of all the states, as there might still be some degree of delocalization or spread in the system. As the value of h increases, the eigenstates gradually become fully localized. The localization property of the eigenstates is again calculated by the IPR, and these are shown by the color coding. Moreover, this formation of loops and their coalescence with the increment of the parameter h indicate an emergence of nontrivial topology in the system, which is identified by a nonzero winding number. Thus Fig. 4(a) itself indicates that the system is simultaneously making three different phase transitions or triple phase transitions. The presence of triple phase transitions is more obvious in Figs. 4(b)–4(e).

In Figure 4(b), we show the real and imaginary parts of the eigenvalues as a function of h, and the corresponding IPR values are shown by the color. All the eigenstates before the critical point ($h < h_c$) are extended, resulting in the robust spectrum for real and imaginary parts of the spectrum. After the critical point, the eigenvalues diverge and become complex. Here, once again, this spectral phase boundary simultaneously marks the transition of $\mathcal{PT}$ symmetry and MI. From the phase diagrams, given in Fig. 2 and Figs. 4(a) and 4(b), we get an indication that, for $\gamma = 0.05$, the system shows the triple phase transition at $h = h_c = 0.68$. We are now going to show this decisively in Figs. 4(c)–4(e). In

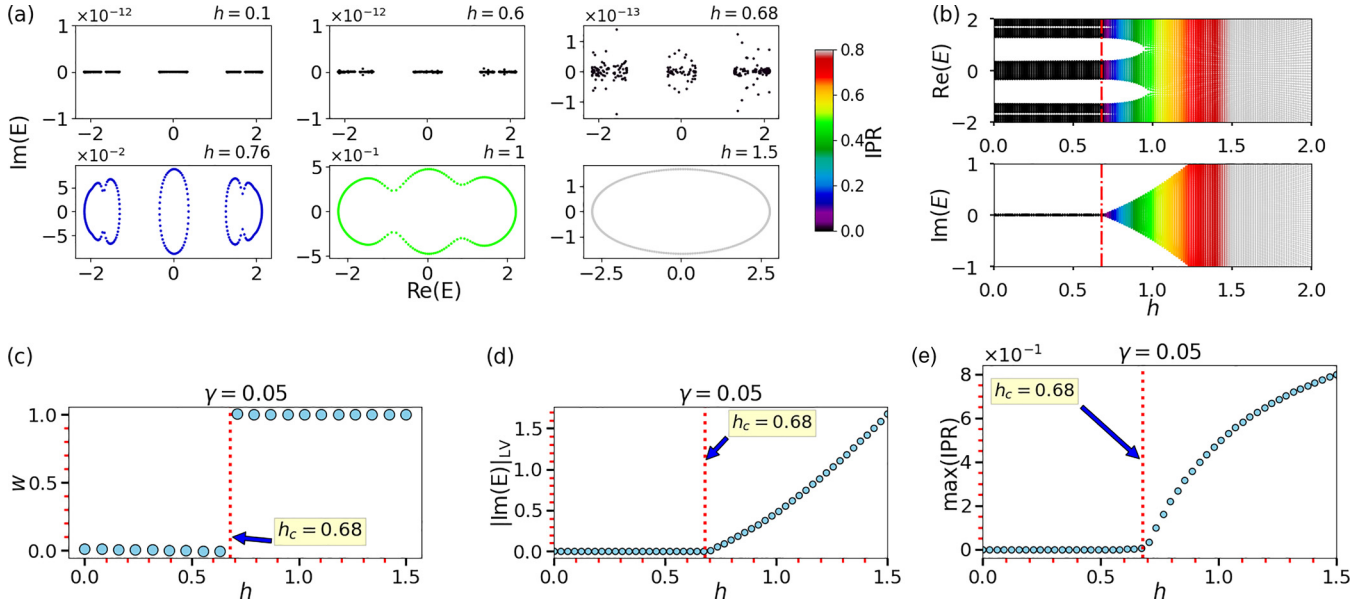

FIG. 4. The figure shows the eigenspectra, MI transition, PT transition, and topological transition by varying the parameter h, for $V = t = 1.0$, and $\gamma = 0.05$. We observe three simultaneous phase transitions. Panel (a) displays the real and imaginary parts of eigenvalues (on the complex plane) and IPRs (in color scale) under the PBC for six typical values of h. With an increase in the value of h, the eigenstates tend to get localized, which is shown by color. We observe that the eigenspectra form a loop for $h > 0.68$, encircling the origin of the complex energy plane, indicating a topologically nontrivial phase with nonzero windings. Also, we observe that the eigenvalues are real for $h < 0.68$, but the $\mathcal{PT}$ symmetry tends to break completely for $h \geqslant 0.68$, and thus we observe complex eigenvalues. Panel (b) shows the real parts of the eigenenergies of the Hamiltonian under PBC, where the overall energy becomes on average constant, for $h < h_c$. The bottom part of the panel displays the imaginary parts of the eigenenergies with increasing h. The color coding is done according to the IPR, where the red-dashed line corresponds to the phase boundary. Panel (c) shows the winding number versus the complex phase shift h. The winding number makes a transition from 0 to 1 as we vary $h < h_c$ to $h > h_c$. Panel (d) represents the largest value of the imaginary part of energy versus the complex phase shift h. For $h < h_c$, the system changes to the unbroken $\mathcal{PT}$ phase, where the spectrum becomes real. For $h > h_c$, there is a broken $\mathcal{PT}$ phase owing to the appearance of complex eigenvalues. Panel (e) represents the maximum value of IPRs contrasted to the complex phase shift h. For $h < h_c$, we observe the delocalized phase, marked by a zero IPR value. For $h > h_c$, all eigenstates become exponentially localized, which is marked by an increase in the IPR value. The length of the lattice is chosen to be $L = 233$ for all the panels.

Fig. 4(c), the topological phase transition is shown by the transition in winding number w. The winding number is computed using Eq. (2). We observe that $w = 0$ when $h < h_c$, and it becomes $w = 1$ for $h \geqslant h_c$. The red dashed line shows the transition point $h_c = 0.68$. Figure 4(d) shows the $\mathcal{PT}$ symmetry transition, which is observed by studying the largest imaginary part of the energy eigenvalues as a function of the complex phase shift h. Here, we again observe $\mathcal{PT}$ symmetry transition at $h_c = 0.68$. Finally, in Fig. 4(e), the maximum value of IPR with respect to h is shown. According to our expectation, here we observe from the behavior of max(IPR) that the system makes the MI transition also at $h_c = 0.68$. These results are in agreement with the phase diagram presented in Fig. 2. Thus we have clearly shown the triple phase transition for $\gamma = 0.05$ at $h_c = 0.68$. Surprisingly, we can control the transitions and can obtain double and sequential phase transitions for this model by simply varying the parameters. We have discussed this point in the SM [40].

V. EXPERIMENTAL REALIZATION

The prototype model, which is studied extensively in this paper, can be simulated in electric circuits using basic components such as capacitors, resistors, inductors, op-amp, etc. [49–51]. In this model, the on-site potential and the hopping between neighboring sites are both non-Hermitian as well as quasiperiodic. In a recent paper, an electrical circuit is proposed to simulate non-Hermitian quasiperiodic on-site potential [52]. An electric circuit design for the quasiperiodic hopping is proposed in another recent paper [53]. Our model can similarly be simulated by combining the above-mentioned electrical circuits.

VI. SUMMARY

We study a non-Hermitian extension of the AAH model, which is $\mathcal{PT}$ symmetric. Here, the non-Hermiticity is considered at the on-site potential, as well as in the nearest-neighbor hopping term. The localization properties of the eigenstates of this model depend strongly on the boundary conditions. The system exhibits primarily localized eigenstates for the open boundary conditions. On the other hand, the MI transition occurs for the periodic boundary conditions. The disorder due to the on-site quasiperiodic potential and the non-Hermitian nature of the system contribute to these boundary-condition-sensitive behaviors. Very importantly, besides the $\mathcal{PT}$ symmetry and the MI transitions, we also observe the topological phase transition in this model. The

overall behaviors of these phases and their transitions are shown via various phase diagrams. Interestingly, these phase diagrams indicate a parameters regime, where we may see the triple phase transition. Later, we decisively show the presence of the triple phase transition or simultaneous transitions of the three phases. Based on some recent proposals, an electric circuit based experimental simulation of this non-Hermitian model is also proposed.

ACKNOWLEDGMENTS

J.N.B. acknowledges financial support from DST-SERB, India through Core Research Grant No. CRG/2020/001701 and also through MATRICS Grant No. MTR/2022/000691. The authors also thank the anonymous referee for her/his valuable comments, which helped in improving the paper.

[1] H. Shen, B. Zhen, and L. Fu, Topological Band Theory for Non-Hermitian Hamiltonians, Phys. Rev. Lett. **120**, 146402 (2018).

[2] E. J. Bergholtz, J. C. Budich, and F. K. Kunst, Exceptional topology of non-Hermitian systems, Rev. Mod. Phys. **93**, 015005 (2021).

[3] A. Ghatak and T. Das, New topological invariants in non-Hermitian systems, J. Phys.: Condens. Matter **31**, 263001 (2019).

[4] K. Kawabata, K. Shiozaki, M. Ueda, and M. Sato, Symmetry and Topology in Non-Hermitian Physics, Phys. Rev. X **9**, 041015 (2019).

[5] Y. Ashida, Z. Gong, and M. Ueda, Non-Hermitian physics, Adv. Phys. **69**, 249 (2020).

[6] C. M. Bender and S. Boettcher, Real Spectra in Non-Hermitian Hamiltonians having $\mathcal{PT}$ Symmetry, Phys. Rev. Lett. **80**, 5243 (1998).

[7] R. El-Ganainy, K. G. Makris, M. Khajavikhan, Z. H. Musslimani, S. Rotter, and D. N. Christodoulides, Non-Hermitian physics and PT symmetry, Nat. Phys. **14**, 11 (2018).

[8] C. M. Bender, M. V. Berry, and A. Mandilara, Generalized PT symmetry and real spectra, J. Phys. A: Math. Gen. **35**, L467 (2002).

[9] H. Wang, X. Zhang, J. Hua, D. Lei, M. Lu, and Y. Chen, Topological physics of non-Hermitian optics and photonics: A review, J. Opt. **23**, 123001 (2021).

[10] X.-S. Li, Z.-Z. Li, L.-L. Zhang, and W.-J. Gong, $\mathcal{PT}$-symmetry of the Su-Schrieffer-Heeger model with imaginary boundary potentials and next-nearest-neighboring coupling, J. Phys.: Condens. Matter **32**, 165401 (2020).

[11] C. Yuce and Z. Oztas, PT symmetry protected non-Hermitian topological systems, Sci. Rep. **8**, 17416 (2018).

[12] L. Jin, P. Wang, and Z. Song, Su-Schrieffer-Heeger chain with one pair of $\mathcal{PT}$-symmetric defects, Sci. Rep. **7**, 5903 (2017).

[13] B. Zhu, R. Lü, and S. Chen, $\mathcal{PT}$ symmetry in the non-Hermitian Su-Schrieffer-Heeger model with complex boundary potentials, Phys. Rev. A **89**, 062102 (2014).

[14] Z. Xu, R. Zhang, S. Chen, L. Fu, and Y. Zhang, Fate of zero modes in a finite Su-Schrieffer-Heeger model with $\mathcal{PT}$ symmetry, Phys. Rev. A **101**, 013635 (2020).

[15] N. Okuma, K. Kawabata, K. Shiozaki, and M. Sato, Topological Origin of Non-Hermitian Skin Effects, Phys. Rev. Lett. **124**, 086801 (2020).

[16] K. Zhang, Z. Yang, and C. Fang, Correspondence between Winding Numbers and Skin Modes in Non-Hermitian Systems, Phys. Rev. Lett. **125**, 126402 (2020).

[17] S. Yao and Z. Wang, Edge States and Topological Invariants of Non-Hermitian Systems, Phys. Rev. Lett. **121**, 086803 (2018).

[18] F. Song, S. Yao, and Z. Wang, Non-Hermitian Topological Invariants in Real Space, Phys. Rev. Lett. **123**, 246801 (2019).

[19] T. E. Lee, Anomalous Edge State in a Non-Hermitian Lattice, Phys. Rev. Lett. **116**, 133903 (2016).

[20] P. W. Anderson, Absence of diffusion in certain random lattices, Phys. Rev. **109**, 1492 (1958).

[21] N. Hatano and D. R. Nelson, Localization Transitions in Non-Hermitian Quantum Mechanics, Phys. Rev. Lett. **77**, 570 (1996).

[22] N. Hatano and D. R. Nelson, Vortex pinning and non-Hermitian quantum mechanics, Phys. Rev. B **56**, 8651 (1997).

[23] N. Hatano, Localization in non-Hermitian quantum mechanics and flux-line pinning in superconductors, Phys. A (Amsterdam, Neth.) **254**, 317 (1998).

[24] P. W. Brouwer, P. G. Silvestrov, and C. W. J. Beenakker, Theory of directed localization in one dimension, Phys. Rev. B **56**, R4333 (1997).

[25] A. F. Tzortzakakis, K. G. Makris, and E. N. Economou, Non-Hermitian disorder in two-dimensional optical lattices, Phys. Rev. B **101**, 014202 (2020).

[26] Y. Huang and B. I. Shklovskii, Anderson transition in three-dimensional systems with non-Hermitian disorder, Phys. Rev. B **101**, 014204 (2020).

[27] K. Kawabata and S. Ryu, Nonunitary Scaling Theory of Non-Hermitian Localization, Phys. Rev. Lett. **126**, 166801 (2021).

[28] X. Luo, T. Ohtsuki, and R. Shindou, Universality Classes of the Anderson Transitions Driven by Non-Hermitian Disorder, Phys. Rev. Lett. **126**, 090402 (2021).

[29] C. Yuce, $\mathcal{PT}$ symmetric Aubry-André model, Phys. Lett. A **378**, 2024 (2014).

[30] Q.-B. Zeng, S. Chen, and R. Lü, Anderson localization in the non-Hermitian Aubry-André-Harper model with physical gain and loss, Phys. Rev. A **95**, 062118 (2017).

[31] D.-W. Zhang, L.-Z. Tang, L.-J. Lang, H. Yan, and S.-L. Zhu, Non-Hermitian topological Anderson insulators, Sci. China Math. **63**, 267062 (2020).

[32] H. Jiang, L.-J. Lang, C. Yang, S.-L. Zhu, and S. Chen, Interplay of non-Hermitian skin effects and Anderson localization in nonreciprocal quasiperiodic lattices, Phys. Rev. B **100**, 054301 (2019).

[33] L.-Z. Tang, G.-Q. Zhang, L.-F. Zhang, and D.-W. Zhang, Localization and topological transitions in non-Hermitian quasiperiodic lattices, Phys. Rev. A **103**, 033325 (2021).

[34] S. Aubry and G. André, Analyticity breaking and Anderson localization in incommensurate lattices, Ann. Isr. Phys. Soc. **3**, 133 (1980).

[35] S. Longhi, Metal-insulator phase transition in a non-Hermitian Aubry-André-Harper model, Phys. Rev. B **100**, 125157 (2019).

[36] S. Longhi, Topological Phase Transition in Non-Hermitian Quasicrystals, Phys. Rev. Lett. **122**, 237601 (2019).

[37] S. Weidemann, M. Kremer, S. Longhi, and A. Szameit, Topological triple phase transition in non-Hermitian Floquet quasicrystals, Nature (London) **601**, 354 (2022).

[38] S. Schiffer, X.-J. Liu, H. Hu, and J. Wang, Anderson localization transition in a robust $\mathcal{PT}$-symmetric phase of a generalized Aubry-André model, Phys. Rev. A **103**, L011302 (2021).

[39] Y. Liu, Q. Zhou, and S. Chen, Localization transition, spectrum structure, and winding numbers for one-dimensional non-Hermitian quasicrystals, Phys. Rev. B **104**, 024201 (2021).

[40] See Supplemental Material at http://link.aps.org/supplemental/10.1103/PhysRevB.108.014204 for details on the PT-symmetry of the model, observation of double and sequential phase transitions, characterization of multi-fractal, extended and localized behavior in the eigenstates, and the Hofstadter butterfly-like fractal energy spectrum.

[41] C. Aulbach, A. Wobst, G.-L. Ingold, P. Hänggi, and I. Varga, Phase-space visualization of a metal–insulator transition, New J. Phys. **6**, 70 (2004).

[42] Z. Gong, Y. Ashida, K. Kawabata, K. Takasan, S. Higashikawa, and M. Ueda, Topological Phases of Non-Hermitian Systems, Phys. Rev. X **8**, 031079 (2018).

[43] X. Cai, Localization and topological phase transitions in non-Hermitian Aubry-André-Harper models with *p*-wave pairing, Phys. Rev. B **103**, 214202 (2021).

[44] Z.-H. Wang, F. Xu, L. Li, D.-H. Xu, and B. Wang, Topological superconductors and exact mobility edges in non-Hermitian quasicrystals, Phys. Rev. B **105**, 024514 (2022).

[45] S. Roy, I. M. Khaymovich, A. Das, and R. Moessner, Multifractality without fine-tuning in a Floquet quasiperiodic chain, SciPost Phys. **4**, 025 (2018).

[46] J. Fraxanet, U. Bhattacharya, T. Grass, M. Lewenstein, and A. Dauphin, Localization and multifractal properties of the long-range Kitaev chain in the presence of an Aubry-André-Harper modulation, Phys. Rev. B **106**, 024204 (2022).

[47] A. J. Martínez, M. A. Porter, and P. Kevrekidis, Quasiperiodic granular chains and Hofstadter butterflies, Philos. Trans. R. Soc. A **376**, 20170139 (2018).

[48] D. R. Hofstadter, Energy levels and wave functions of Bloch electrons in rational and irrational magnetic fields, Phys. Rev. B **14**, 2239 (1976).

[49] C. H. Lee, S. Imhof, C. Berger, F. Bayer, J. Brehm, L. W. Molenkamp, T. Kiessling, and R. Thomale, Topolectrical circuits, Commun. Phys. **1**, 39 (2018).

[50] J. Dong, V. Juričić, and B. Roy, Topolectric circuits: Theory and construction, Phys. Rev. Res. **3**, 023056 (2021).

[51] T. Helbig, T. Hofmann, S. Imhof, M. Abdelghany, T. Kiessling, L. W. Molenkamp, C. H. Lee, A. Szameit, M. Greiter, and R. Thomale, Generalized bulk–boundary correspondence in non-Hermitian topolectrical circuits, Nat. Phys. **16**, 747 (2020).

[52] Q.-B. Zeng and Y. Xu, Winding numbers and generalized mobility edges in non-Hermitian systems, Phys. Rev. Res. **2**, 033052 (2020).

[53] Q.-B. Zeng, Y.-B. Yang, and Y. Xu, Topological phases in non-Hermitian Aubry-André-Harper models, Phys. Rev. B **101**, 020201(R) (2020).